Self-Alignment of Pd_8 Chains

DOI: 10.1002/anie.201409511

Self-Alignment of Low-Valent Octanuclear Palladium Atoms**

*Kanako Nakamae, Yukie Takemura, Bunsho Kure, Takayuki Nakajima, Yasutaka Kitagawa, and Tomoaki Tanase**

Abstract: *A linear tetraphosphine, meso-bis[(diphenylphosphinomethyl)phenylphosphino]methane (dpmppm) was used to synthesize linear octapalladium-extended metal atom chains as discrete molecules of $[Pd_8(\mu\text{-dpmppm})_4](BF_4)_4$ (**1**) and $[Pd_8(\mu\text{-dpmppm})_4L_2](BF_4)_4$ (L = 2,6-xylyl isocyanide (XylNC; **2**), acetonitrile (**3**), and N,N-dimethylformamide (dmf; **4**)), which are stable in the solution states and show interesting temperature-dependent photochemical properties in the near IR region. Variable temperature NMR studies demonstrated that at higher temperature $T \approx 140\,^{\circ}C$ the Pd_8 chains were dissociated into Pd_4 fragments, which were thermodynamically self-aligned to restore the Pd_8 chains at lower temperature $T < 60\,^{\circ}C$. The coldspray ionization mass spectra suggested a possibility for further aggregation of the linear tetrapalladium units.*

Metallic materials have widely been utilized in a variety of electronic devices, and their downsizing into nanoscaled fabricates is extremely desired in modern industries from the viewpoint of saving energy and resources to establish sustainable future systems.[1] Among the motifs of nanostructures, one-dimensional arrays of metal atoms (*meso*- to nanowires) have attracted rapidly growing attention as nanoscaled multifunctional devices. This has been promoted by the synthetic developments, e.g., the electrodeposition of metal atoms on step-edges of crystalline substrates into nanochannels and between nanogaps as well as physical manipulations with scanning probe microscopy, electron-beam lithography, and break junction techniques.[2] Along this line, the ultimately thinnest electric wire that may consist of a single-metal-atom chain sheathed with insulating materials, so-called "extended metal atom chains" (EMACs), is one of the most theoretically important and challenging targets, because the anisotropically confined electrons in a single metallic chain would be predicted to exhibit fundamentally different transport properties, conceptually corresponding to the transition from atomic to bulk electronic behavior.

Although their reproducible synthesis is extremely difficult at present, one of the promising strategies involves a procedure of molecular chemistry that constructs linearly ordered multinuclear metal complexes as discrete molecular EMACs. Several groups have synthesized molecular EMACs by using linearly well-designed multidonor organic ligands as guiding templates,[3–14] establishing Ni_9 and Ni_{11} chains supported by polypyridyl- and polynaphthyridylamide ligands, respectively, as the longest end of structurally characterized examples.[9,10] These compounds are promising building blocks for extending the metal atom chains, whereas the length of the molecular EMACs is still quite limited and entirely depends on the length of the organic ligands. We have studied linearly ordered metal complexes supported by a triphosphine, bis(diphenylphosphinomethyl)phenylphosphine (dpmp), and reported that linear Pt_2M trinuclear complexes, $[Pt_2M(\mu\text{-dpmp})_2L_2]^{2+}$ (M = Pt, Pd, L = isocyanide), were reductively coupled to form hydride-bridged $Pt_2M_2Pt_2$ hexanuclear complexes, $[Pt_4M_2(\mu\text{-H})(\mu\text{-dpmp})_4L_2]^{3+}$, which were further transformed to the $Pt_2M_2Pt_2$ chains by two-electron oxidation.[15] These kinetically controlled procedures implied that the incremental expansion of linear multinuclear building blocks is applicable for the preparation of discrete molecular EMACs. To increase the number of metal atoms, we have recently developed a linear tetraphosphine, *meso*-bis[(diphenylphosphinomethyl)phenylphosphino]methane (dpmppm),[16] and tried to synthesize extended metal atom chains at a low oxidation state, which could be an atomic replica of real electric wires. In the present study, we have discovered that tetrapalladium fragments supported by two dpmppm ligands, $\{Pd_4(\mu\text{-dpmppm})_2\}^{2+}$, are thermodynamically self-aligned into a linear octapalladium array of $\{Pd_8(\mu\text{-dpmppm})_4\}^{4+}$ in the solution state. The electronic properties of the octapalladium chains are tuned by a series of terminal capping ligands, and the coldspray ionization (CSI) mass spectra indicated the possibility of further aggregation of the tetrapalladium units that could lead to unit-incremental expansions of palladium wires.

When the tetraphosphine dpmppm (in dichloromethane) was reacted with $[Pd(dba)_2]$ and $[Cu(CH_3CN)_4]BF_4$[17] in a ratio of 1:2:1, an octanuclear palladium complex, formulated as $[Pd_8(\mu\text{-dpmppm})_4](BF_4)_4$ (**1**), was obtained in a crystalline form (Scheme 1). Complex **1** was coordinatively unsaturated without terminal capping ligands, and its cluster

[*] K. Nakamae, Dr. Y. Takemura, Dr. B. Kure, Prof. T. Nakajima, Prof. T. Tanase
Department of Chemistry, Faculty of Science
Nara Women's University
Kitauoya-nishi-machi, Nara, 630-8506 (Japan)
E-mail: tanase@cc.nara-wu.ac.jp
Prof. Y. Kitagawa
Department of Materials Engineering Science
Graduate School of Engineering Science, Osaka University
1-3 Machikaneyama, Toyonaka, Osaka 560-8531 (Japan)

[**] This work was supported by Grants-in-Aid for Scientific Research and that on Priority Area 2107 (nos. 22108521, 24108727, 22108515, 24108721) from the Ministry of Education, Science, Sports, and Culture of Japan. The authors thank Prof. Kohtaro Osakada, Dr. Makoto Tanabe, and Mr. Masato Koizumi of Tokyo Institute of Technology for their help in CSI-TOF mass spectrometry. T.T. is grateful to Nara Women's University for a research project grant. K.N. is grateful for a JSPS fellowship.

Supporting information for this article is available on the WWW under http://dx.doi.org/10.1002/anie.201409511.

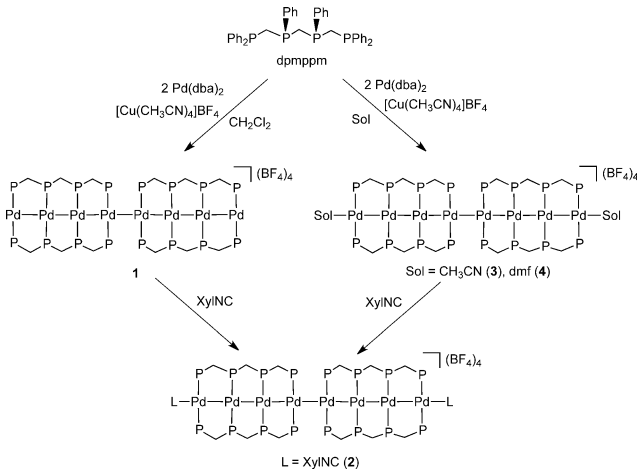

Scheme 1. Preparation of octapalladium complexes **1**–**4**.

valence electron count (CVE) of 108 is six-electron-deficient from the electron precise number of 114 which corresponds to eight $16e^-$ Pd centers linearly connected by metal–metal covalent bonds, and consequently, complex **1** readily reacted with 2,6-xylyl isocyanide (XylNC) to afford $[Pd_8(\mu\text{-dpmppm})_4(XylNC)_2](BF_4)_4$ (**2**; CVE 112). When similar reactions were carried out in acetonitrile (CH_3CN) or *N*,*N*-dimethylformamide (dmf), solvent-terminated octanuclear palladium complexes, $[Pd_8(\mu\text{-dpmppm})_4L_2](BF_4)_4$ (L = CH_3CN (**3**), dmf (**4**)), were isolated as crystals (Scheme 1).

The detailed structures of **1**–**4** were determined by X-ray crystallography (Figures 1 a–c, S1–S4, and Tables S1–S3)[18] to consist of linearly aligned octapalladium atoms (Pd-Pd-Pd = 174.42–179.50°) bridged by four dpmppm ligands and terminated without (**1**) and with σ-donating organic molecules of XylNC (**2**), CH_3CN (**3**), and dmf (**4**). The complex cations have +4 charge, neutralized with four BF_4^- anions, indicating that the average oxidation state of Pd is +0.5 with apparent involvement of Pd^0 atoms in a chain. Notably, the octanuclear chain is the longest discrete molecular EMAC of low-valent precious metals thus far, whereas it should be noted that Ritter et al. reported solution-stable one-dimensional Pd(+3)

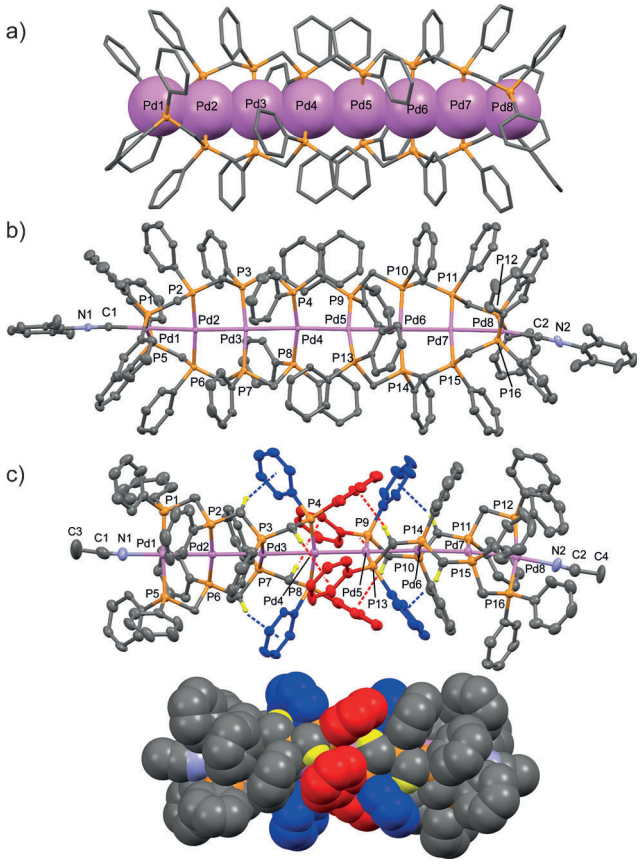

Figure 1. a) Perspective view of the complex cation of **1**, with space filling diagrams for Pd and capped stick models for P and C atoms. b) ORTEP diagram for the complex cation of **2**. c) ORTEP diagram for the complex cation of **3**, in which C–H–π interactions are highlighted with red and blue colored phenyl groups (c, top) and a perspective view drawn with space filling models (c, bottom).

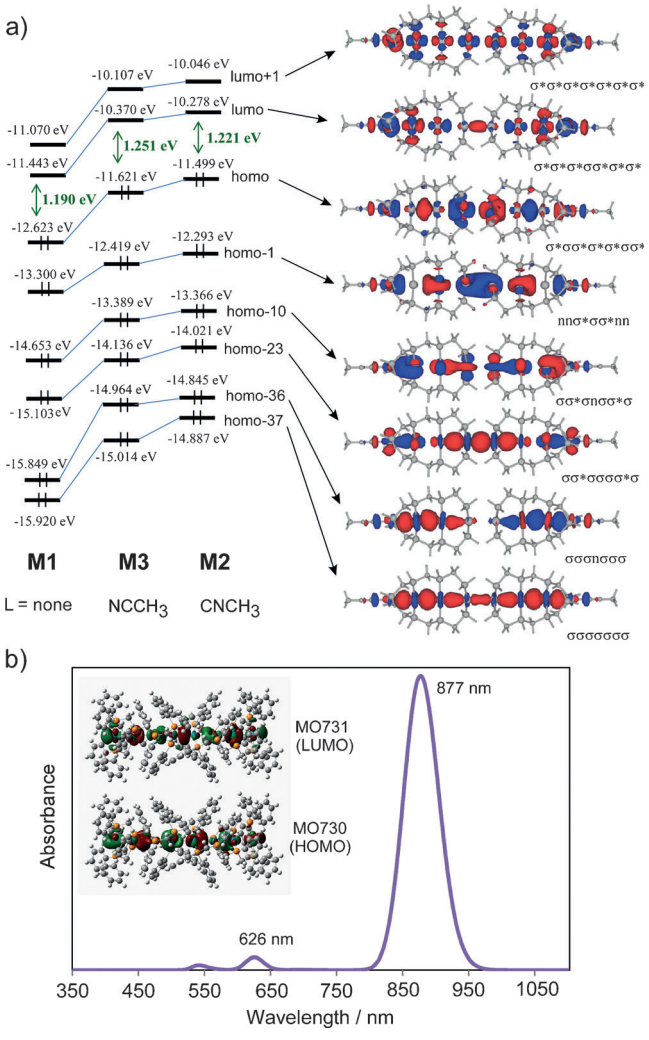

Figure 2. a) Plots of MOs responsible for σ-interactions in the Pd_8 strings for the model compounds, $[Pd_8(C_3H_{12}P_4)_4]^{4+}$ (**M1**), $[Pd_8(C_3H_{12}P_4)_4(CNCH_3)_2]^{4+}$ (**M2**), and $[Pd_8(C_3H_{12}P_4)_4(NCCH_3)_2]^{4+}$ (**M3**), optimized by DFT calculations. b) A simulated absorption spectrum for **1** by TD-DFT calculations, and plots of HOMO and LUMO for the real structure of **1** (inset views).

and Pd(+2.5) wires characterized as molecular-weight-distributed coordination polymers in the solutions.[19] The Pd–Pd distances ranging from 2.6249(6) to 2.7921(6) Å suggest that all Pd atoms are connected with metal–metal bonding interactions and show an ideal D_2 symmetrical structure, in which the Pd–Pd distances become longer from the outside to the inside part. Interestingly, the central Pd–Pd distances with no bridging ligand were shorter than the neighboring Pd–Pd distances, as Pd_{out}–Pd_{in} (2.625–2.693 Å) < Pd_{in}–$Pd_{in'}$ (2.682–2.733 Å) < $Pd_{in'}$–Pd_{cen} (2.765–2.792 Å) > Pd_{cen}–Pd_{cen} (2.732–2.774 Å) for the {$Pd_{out}Pd_{in}Pd_{in'}Pd_{cen}Pd_{cen}Pd_{in'}Pd_{in}Pd_{out}$} array. Furthermore, the complex cations of **1**–**4** exhibit four inter- and four intraligand C–H–π interactions between the phenyl groups and the methylene C–H units of dpmppm ligands (Figures 1c, S1–S4, and Tables S4–S7); the former may play an important role in supporting the central Pd–Pd bonding interaction, because it has no bridging ligand (Figure 1c, phenyl groups shown in red).

To examine Pd–Pd bonding nature, gas phase theoretical optimizations with DFT methods (B3LYP/LANL2DZ)[20] were performed on the model compounds $[Pd_8(C_3H_{12}P_4)_4]^{4+}$ (**M1**), $[Pd_8(C_3H_{12}P_4)_4(CNCH_3)_2]^{4+}$ (**M2**), and $[Pd_8(C_3H_{12}P_4)_4(NCCH_3)_2]^{4+}$ (**M3**), which correspond to the real structures of **1**, **2**, and **3**, respectively, though the phenyl groups of the dpmppm ligands were replaced with H atoms (Figures S14–S15 and Table S8). The optimized structures are basically in agreement with the crystal structures besides systematic increases of the Pd–Pd distances. The eight crucial molecular orbitals (MOs) responsible for σ-interactions of d-, s-, and p-hybridized Pd orbitals are assigned as illustrated in Figure 2a; the HOMO consists of an antibonding interaction between the two central Pd atoms and the LUMO is composed of a bonding interaction between them. Upon introducing the terminal ligands, $NCCH_3$ and $CNCH_3$ to **M1**, the energy levels of HOMO and LUMO increase in a parallel fashion, resulting in slight changes of the HOMO–LUMO gaps. The Wiberg bond indices (WBIs)[21] indicate that metal–metal single bonds exist between the Pd_{out}–Pd_{in} (WBIs = 0.380–0.414) and Pd_{in}–$Pd_{in'}$ (WBIs = 0.331–0.374) pairs. On the other hand, bonding interactions between the four inner Pd atoms ($Pd_{in'}$–Pd_{cen}–Pd_{cen}–$Pd_{in'}$) are weak and delocalized as WBIs are 0.223–0.254 for Pd_{in}–Pd_{cen} and 0.175–0.183 for Pd_{cen}–Pd_{cen}, suggesting that four σ-bonding electrons are delocalized in between the central four Pd atoms (Figure S15 and Table S8). The WBI analysis with single-point DFT calculations on the real structure of **1** also showed the similar delocalized bonding interactions between the central four Pd atoms, which should be a main factor in constructing the Pd_8 chains (Table S9).

The octapalladium chains of **1**–**4** are remarkably stable in the solution states at room temperature and exhibit interesting temperature-dependent phenomena. The electronic absorption spectra of **1** and **2** in CH_2Cl_2 at 25 °C (Figure 3a and b) showed a characteristic band at 967 nm (**1**) and 941 nm (**2**), together with absorptions at 669 nm (**1**) and 652 nm (**2**). When the temperature decreased to −60 °C, the intensity of the NIR absorption bands dramatically increased at 954 nm (**1**) and 929 nm (**2**) and contrary, the peaks of the higher energy absorptions around 650–670 nm disappeared; the spectral changes occurred in a perfectly reversible way. To assign the characteristic absorptions of **1** (954 nm at −60 °C) and **2** (929 nm at −60 °C), TD-DFT (TD = time-dependent) calculations[22] were carried out on the real structures of **1** and **2** by using restricted (*R*)-B3LYP functionals with a basis set of LANL2DZ for Pd, 6-31 + G* for P, 6-31G* for C, and 6-31G for H as single-point calculations, and showed very intense absorptions at 877 nm with *f* (oscillator strength) = 1.750 for **1** and at 888 nm with *f* = 2.294 for **2**, which are exclusively assignable to spin-allowed HOMO–LUMO transitions (Figures 2b and S16–S19). As to the higher energy absorptions at 669 nm (**1**) and 652 nm (**2**) at 25 °C, the TD-DFT calculations did not show meaningful peaks.[23]

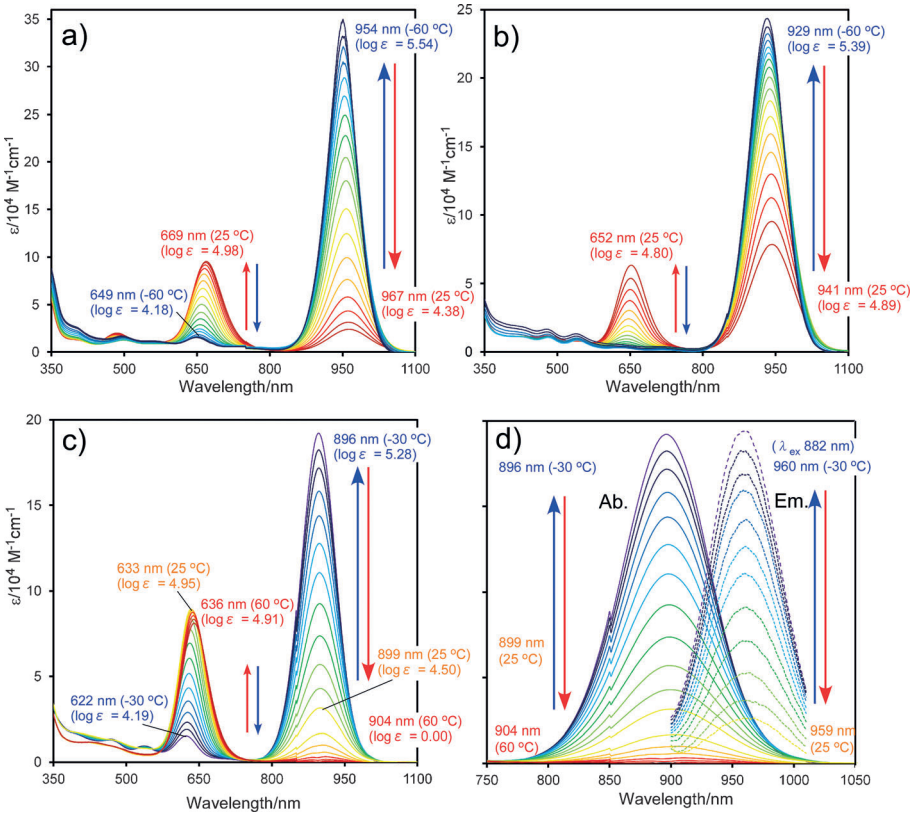

Figure 3. Temperature-dependent electronic absorption spectra of **1** (a) and **2** (b) in CH_2Cl_2 and **3** (c) in CH_3CN. d) Temperature-dependent absorption (Ab. left) and emission (Em. right, excited at 882 nm) spectra of **3** in CH_3CN for the near IR region.

The solvent-terminated complexes **3** and **4** are extremely stable in the respective solvent, and also exhibited the temperature-dependent characteristic absorption spectral changes (Figures 3c and S5); the intensities of NIR absorptions increase at low temperature at 896 nm (**3**, −30 °C) and 910 nm (**4**, −50 °C), whereas they decrease at room temperature and disappeared at higher temperature. Complex **3** is interestingly luminous to emit at 960 nm (−30 °C) upon an irradiation at 882 nm in acetonitrile with a temperature dependency similar to the absorption band (Figure 3d). The small Stokes shift of 744 cm^{-1} suggested that the photo-induced structural changes between the ground and excited states are remarkably small, which may be attributed to the interligand C–H–π interactions at lower temperature (see below). In other words, the quite intense NIR absorption at low temperature is presumed to bear a character of 0–0 transition in the vibrational mode with respect to the central Pd–Pd bond on considering vibrational overlap Frank–Condon factor.[24] It should be noted that the HOMO–LUMO transition energy of **1**–**4** derived from the NIR absorption at low temperature [10.48 (**1**), 10.76 (**2**), 10.98 (**3**), 10.99 kcm^{-1} (**4**)] showed an approximate positive correlation to the Pd_{cen}–Pd_{cen} distances [2.7319(6) (**1**), 2.7391(6) (**2**), 2.7575(6) (**3**), 2.7743(4) Å (**4**)] determined by X-ray analyses, demonstrating that the electronic structures of the Pd_8 chains can be tuned by varying the terminal ligands. The $^1H\{^{31}P\}$ NMR spectrum of **3** in CD_3CN at room temperature exhibited six doublets for the methylene protons of dpmppm ligands, two of which were significantly low-energy-shifted at δ 0.86 and 1.02 ppm due to ring current effects of the phenyl groups involved in C–H–π interactions (Figure 4a left). When the temperature varied from −30 °C to 60 °C, the doublets gradually moved to higher field with somewhat broadening features. The $^{31}P\{^1H\}$ NMR spectrum of **3** in CD_3CN showed well-resolved four resonances at δ 2.55, −6.14, −9.01, and −15.56 ppm in a 1:1:1:1 ratio, which were assigned to the P nuclei coordinating to the Pd_{cen}, Pd_{out}, $Pd_{in'}$, and Pd_{in}, respectively, by using ^{31}P–^{31}P COSY and ^{31}P–^1H HMBC NMR techniques (Figures 4a right and S6–S8). The spectral patterns are almost unchanged upon varying the temperature, only exhibiting a broadening feature at 60 °C. These NMR spectra suggested that the solvent-terminated octapalladium chain is retained even in the solution, and is effectively supported at low temperature by interligand C–H–π interactions as are found in the solid state structure, whereas they may be weakened to some extent at higher temperature around 60 °C.

The $^{31}P\{^1H\}$ and $^1H\{^{31}P\}$ NMR spectra of **4** in $[D_7]$DMF below 60 °C showed similar spectral patterns to those observed for **3** (Figures 4b, S9, and S10); however, at higher temperature $60 < T < 140$ °C, the spectral changes demonstrated another dynamic behavior relating to its dissociation into tetrapalladium units. In the $^{31}P\{^1H\}$ NMR spectra (Figure 4b), the four peaks coalesced to two resonances (T_c

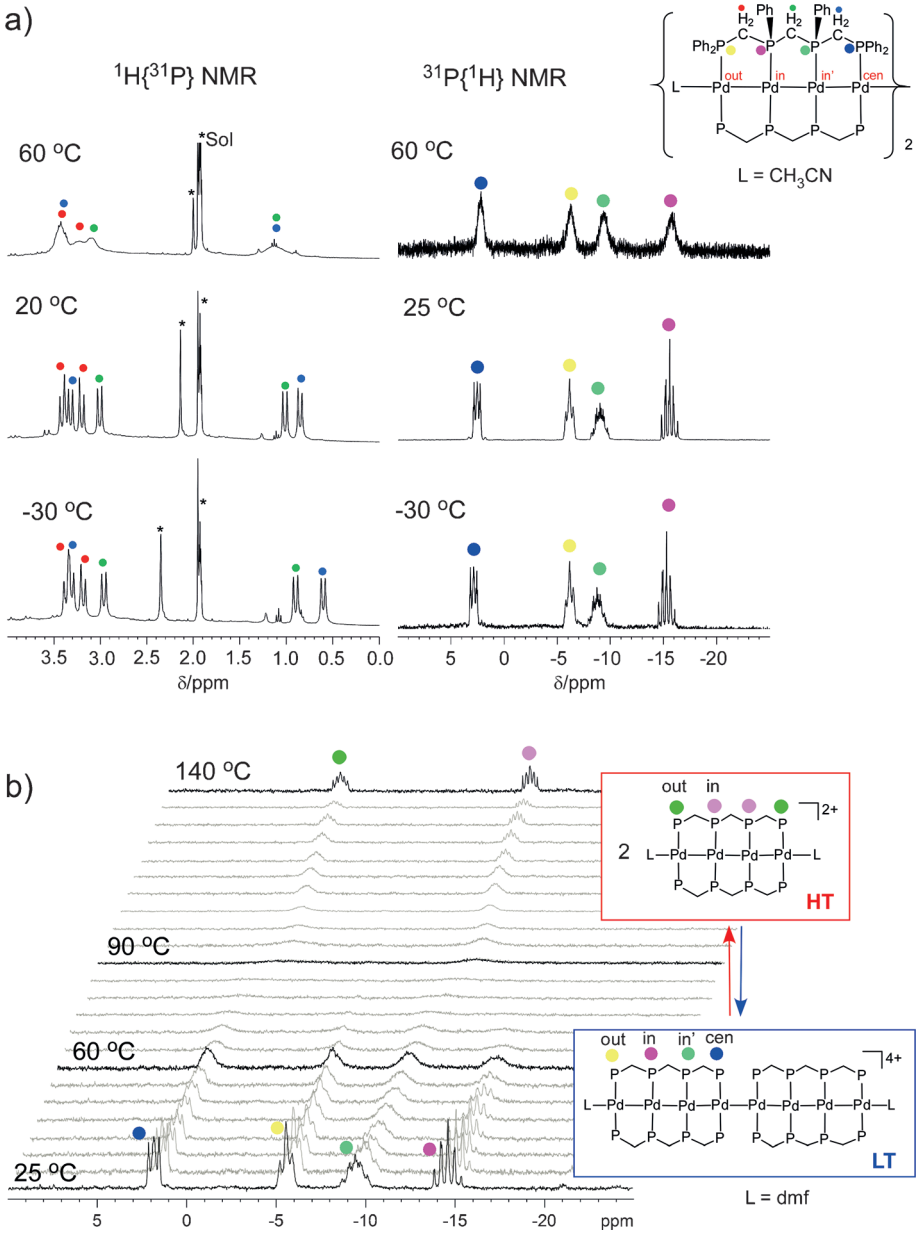

Figure 4. a) Temperature-dependent $^1H\{^{31}P\}$ NMR (left) and $^{31}P\{^1H\}$ NMR (right) spectra of **3** in CD_3CN and their assignments. b) Temperature-dependent $^{31}P\{^1H\}$ NMR spectra of **4** in $[D_7]$DMF and their assignments.

≈85 °C), which became well resolved at δ 0.4 and −10.3 ppm in a 1:1 ratio at 140 °C. In the $^1H\{^{31}P\}$ NMR spectrum at 140 °C, the peaks for the methylene protons of dpmppm ligands appeared symmetrically at δ 4.09, 3.97, 3.73, and 2.76 ppm in a 1:2:2:1 ratio without any low-energy shifts due to C–H–π interactions (Figure S11). These symmetrical spectra are consistent with a solvent-capped symmetrical tetrapalladium structure of $[Pd_4(\mu\text{-dpmppm})_2(dmf)_2]^{2+}$ (**5**), by analogy with the isocyanide-terminated tetrapalladium complexes.[16c] The $^{31}P\{^1H\}$ NMR spectral changes occurred reversibly to reveal an equilibrium in which the Pd_8 complex **4** is the major species below ca. 60 °C and the Pd_4 complex **5** is the major species at around 140 °C, providing estimated thermodynamic parameters of $\Delta H^o = 44(3)$ kcal mol^{-1} and $\Delta S^o = 120(8)$ cal mol^{-1} K^{-1} (Figure S20). From the thermodynamic data, the Pd_8 and Pd_4 species exist in a ca. 1:1 ratio around 90 °C. In other words, the two $\{Pd_4(\mu\text{-dpmppm})_2\}^{2+}$ units were thermodynamically self-aligned below ca. 60 °C to restore the Pd_8 chain of $\{Pd_8(\mu\text{-dpmppm})_4\}^{4+}$.

The coldspray ionization (CSI) mass spectra of **3** in CH_3CN were measured to elucidate the solution species (Figures S12 and S13). Unfortunately, the main intense peaks were observed at $m/z = 840.929$ ($z = 2$) and 1768.867 ($z = 1$), corresponding to $[Pd_4(dpmppm)_2]^{2+}$ (840.986) and $\{[Pd_4(dpmppm)_2]BF_4\}^+$ (1768.976), which were generated by fragmentation of **3** during the ionization processes, but a closer investigation of the higher mass number region ($2000 < m/z < 6000$) disclosed a series of peaks for species of higher nuclearity derived from aggregation of $\{Pd_4(dpmppm)_2\}^{2+}$ units, including distinct peaks at $m/z =$ 3625.646 ($z = 1$), 2697.337 ($z = 2$), 2388.135 ($z = 3$), and 3007.453 ($z = 3$), which were unambiguously assigned to $\{[Pd_8(dpmppm)_4](BF_4)_3\}^+$ ($m/z = 3625.956$), $\{[Pd_{12}(dpmppm)_6](BF_4)_4\}^{2+}$ ($m/z = 2697.467$), $\{[Pd_{16}(dpmppm)_8](BF_4)_5\}^{3+}$ ($m/z = 2388.970$), and $\{[Pd_{20}(dpmppm)_{10}](BF_4)_7\}^{3+}$ ($m/z = 3007.297$) by simulating the distributions of isotopomers (Figure S13a–c). Although their intensities were generally very weak and the higher-nuclearity species might be generated during the ionization processes, the series of CSI-MS peaks implied the possibility of further incremental extension of palladium chains by aggregation of the tetrapalladium units.

In summary, a series of linear octapalladium clusters was successfully synthesized through thermodynamic self-alignment of two $\{Pd_4(\mu\text{-dpmppm})_2\}^{2+}$ units by utilizing the tetraphosphine dpmppm. The octapalladium chains are stable in the solutions and exhibited interesting temperature-dependent photochemical properties, which were tuned by varying the terminal capping ligands. The present findings are quite useful for establishing nanostructured metal strings by bottom-up constructions making use of linear metallic building blocks.

Received: September 26, 2014
Revised: October 29, 2014
Published online: November 24, 2014

Keywords: metal atom chains · octanuclear complexes · palladium · self-assembly · tetraphosphines

[1] C. S. S. R. Kumar in *Metallic Nanomaterials*, Wiley-VCH, Weinheim, **2009**.

[2] a) "Atomic Chains at Surface" J. E. Ortega, F. J. Himpsel in *Very High Resolution Photoelectron Spectroscopy* (Ed.: S. Hüfner), Springer, Berlin, **2007**, pp. 147–183; b) F. Favier, E. C. Walter, M. P. Zach, T. Benter, R. M. Penner, *Science* **2001**, *293*, 2227–2231; c) S. R. Bahn, K. W. Jacobsen, *Phys. Rev. Lett.* **2001**, *87*, 266101; d) P. Gambardella, A. Dallmeyer, K. Maiti, M. C. Malagoli, W. Eberhardt, K. Kern, C. Carbone, *Nature* **2002**, *416*, 301–304; e) M. A. Bangar, K. Ramanathan, M. Yun, C. Lee, C. Hangarter, N. V. Myung, *Chem. Mater.* **2004**, *16*, 4955–4959; f) D. M. Tang, L.-C. Yin, F. Li, C. Liu, W.-J. Yu, P.-X. Hou, B. Wu, Y.-H. Lee, X.-L. Ma, H.-M. Cheng, *Proc. Natl. Acad. Sci. USA* **2010**, *107*, 9055–9059; g) C. Wang, Y. Hu, C. M. Lieber, S. Sun, *J. Am. Chem. Soc.* **2008**, *130*, 8902–8903; h) C. Zhu, H.-C. Peng, J. Zeng, J. Liu, Z. Gu, Y. Xia, *J. Am. Chem. Soc.* **2012**, *134*, 20234–20237; i) B. Y. Xia, H. B. Wu, Y. Yan, X. W. Lou, X. Wang, *J. Am. Chem. Soc.* **2013**, *135*, 9480–9485.

[3] J. F. Berry in *Multiple Bond between Metal Atoms*, 3rd ed. (Eds.: F. A. Cotton, C. A. Murillo, R. A. Walton), Springer, New York, **2005**, pp. 669–706, and references therein.

[4] C.-Y. Yeh, C.-C. Wang, C.-H. Chen, S.-M. Peng in *Redox Systems Under Nano-Space Control* (Ed.: T. Hirao), Springer, Berlin, **2006**, pp. 85–117.

[5] J. K. Bera, K. R. Dunbar, *Angew. Chem. Int. Ed.* **2002**, *41*, 4453–4457; *Angew. Chem.* **2002**, *114*, 4633–4637.

[6] M. Majumdar, J. K. Bera in *Macromolecules Containing Metal and Metal-Like Elements*, *Vol. 9* (Eds.: A. S. A.-E. Aziz, C. E. Carraher, Jr., C. U. Pittman Jr., M. Zeldin), Wiley, Hoboken, **2009**, pp. 181–253.

[7] J. F. Berry in *Structure and Bonding*, *Vol. 136* (Ed.: G. Parkin), Springer, Berlin, **2010**, pp. 1–28.

[8] V. P. Georgiev, P. J. Mohan, D. DeBrincat, J. E. McGrady, *Coord. Chem. Rev.* **2013**, *257*, 290–298.

[9] S.-M. Peng, C.-C. Wang, Y.-L. Jang, Y.-H. Chen, F.-Y. Li, C.-Y. Mou, M.-K. Leung, *J. Magn. Magn. Mater.* **2000**, *209*, 80–83.

[10] R. H. Ismayilov, W.-Z. Wang, G.-H. Lee, C.-Y. Yeh, S.-A. Hua, Y. Song, M.-M. Rohmer, M. Benard, S.-M. Peng, *Angew. Chem. Int. Ed.* **2011**, *50*, 2045–2048; *Angew. Chem.* **2011**, *123*, 2093–2096.

[11] T. Murahashi, E. Mochizuki, Y. Kai, H. Kurosawa, *J. Am. Chem. Soc.* **1999**, *121*, 10660–10661.

[12] T. Murahashi, M. Fujimoto, M. Oka, Y. Hashimoto, T. Uemura, Y. Tatsumi, Y. Nakao, A. Ikeda, S. Sakaki, H. Kurosawa, *Science* **2006**, *313*, 1104–1107.

[13] Y. Tatsumi, T. Murahashi, M. Okada, S. Ogoshi, H. Kurosawa, *Chem. Commun.* **2008**, 477–479.

[14] T. Murahashi, K. Shirato, A. Fukushima, K. Takase, T. Suenobu, S. Fukuzumi, S. Ogoshi, H. Kurosawa, *Nat. Chem.* **2012**, *4*, 52–58.

[15] a) E. Goto, R. A. Begum, S. Zhan, T. Tanase, K. Tanigaki, K. Sakai, *Angew. Chem. Int. Ed.* **2004**, *43*, 5029–5032; *Angew. Chem.* **2004**, *116*, 5139–5142; b) E. Goto, R. A. Begum, A. Hosokawa, C. Yamamoto, B. Kure, T. Nakajima, T. Tanase, *Organometallics* **2012**, *31*, 8482–8497; c) E. Goto, R. A. Begum, C. Ueno, A. Hosokawa, C. Yamamoto, K. Nakamae, B. Kure, T. Nakajima, T. Kajiwara, T. Tanase, *Organometallics* **2014**, *33*, 1893–1904.

[16] a) Y. Takemura, H. Takenaka, T. Nakajima, T. Tanase, *Angew. Chem. Int. Ed.* **2009**, *48*, 2157–2161; *Angew. Chem.* **2009**, *121*, 2191–2195; b) Y. Takemura, T. Nishida, B. Kure, T. Nakajima, M. Iida, T. Tanase, *Chem. Eur. J.* **2011**, *17*, 10528–10532; c) T. Tanase, S. Hatada, A. Mochizuki, K. Nakamae, B. Kure, T. Nakajima, *Dalton Trans.* **2013**, *42*, 15941–15952; d) T. Tanase, R. Otaki, T. Nishida, H. Takenaka, Y. Takemura, B. Kure, T. Nakajima, Y. Kitagawa, T. Tsubomura, *Chem. Eur. J.* **2014**, *20*, 1577–1596.

[17] The Cu^{I} complex $[Cu(CH_3CN)_4]BF_4$ worked as an oxidant to generate Pd^{I} species, which was confirmed by the deposition of metallic copper from the reaction solution. The redox condensation methods have been used to create platinum, rhodium, and iridium linear complexes. See, a) C. Tejel, M. A. Ciriano, L. A. Oro, *Chem. Eur. J.* **1999**, *5*, 1131 – 1135; b) C. Tejel, M. A. Ciriano, B. E. Villarroya, R. Gelpi, J. A. López, F. J. Lahoz, L. A. Oro, *Angew. Chem. Int. Ed.* **2001**, *40*, 4084 – 4086; *Angew. Chem.* **2001**, *113*, 4208 – 4210; c) C. Tejel, M. A. Ciriano, B. E. Villarroya, J. A. López, F. J. Lahoz, L. A. Oro, *Angew. Chem. Int. Ed.* **2003**, *42*, 529 – 532; *Angew. Chem.* **2003**, *115*, 547 – 550; d) B. E. Villarroya, C. Tejel, M.-M. Rohmer, L. A. Oro, M. A. Ciriano, M. Bénard, *Inorg. Chem.* **2005**, *44*, 6536 – 6544; e) M. P. del Río, J. A. López, M. A. Ciriano, C. Tejel, *Chem. Eur. J.* **2013**, *19*, 4707 – 4711, and references therein.

[18] CCDC 1023572 (**1**), 1023573 (**2**), 1023574 (**3**), and 1023575 (**4**) contain the supplementary crystallographic data for this paper. These data can be obtained free of charge from The Cambridge Crystallographic Data Centre via www.ccdc.cam.ac.uk/data_request/cif.

[19] M. G. Campbell, D. C. Powers, J. Raynaud, M. J. Graham, P. Xie, E. Lee, T. Ritter, *Nat. Chem.* **2011**, *3*, 949 – 953.

[20] a) A. D. Becke, *Phys. Rev. A* **1988**, *38*, 3098 – 3100; b) C. Lee, W. Yang, R. G. Parr, *Phys. Rev. B* **1988**, *37*, 785 – 789; c) B. Miehlich, A. Savin, H. Stoll, H. Preuss, *Chem. Phys. Lett.* **1989**, *157*, 200 – 206; d) A. D. Becke, *J. Chem. Phys.* **1993**, *98*, 5648 – 5652.

[21] a) K. B. Wiberg, *Tetrahedron* **1968**, *24*, 1083 – 1096; b) A. E. Reed, L. A. Curtiss, F. Weinhold, *Chem. Rev.* **1988**, *88*, 899 – 926.

[22] M. E. Casida, C. Jamorski, K. C. Casida, D. R. Salahub, *J. Chem. Phys.* **1998**, *108*, 4439 – 4449.

[23] To assign the higher-energy absorptions around 650–670 nm, further detailed theoretical calculations by using Broken-Symmetry (BS)-B3LYP as well as R-B3LYP are in progress.

[24] N. J. Turro, V. Ramamurthy, J. C. Scaiano in *Principles of Molecular Photochemistry—An Introduction*, University Science Books, Sausalito California, **2009**.

